Applied Catalysis B: Environmental 338 (2023) 122985

Contents lists available at ScienceDirect

Applied Catalysis B: Environmental

journal homepage: www.elsevier.com/locate/apcatb

Unraveling the regulation of Mn in Cu-ZnO_x formation during methanol synthesis from syngas over $Cu/ZnO/Al_2O_3$-Mn catalysts

Zhenzhou Zhang [a,1], Sifan Cheng [a,1], Wenqi Liu [a], Baojian Chen [a], Xinhua Gao [b], Peng Wang [c], Jian Gao [a], Yisheng Tan [d], Shanshan Dang [a], Weifeng Tu [a,*]

[a] Engineering Research Center of Advanced Functional Material Manufacturing of Ministry of Education, School of Chemical Engineering, Zhengzhou University, Zhengzhou 450001, China
[b] State Key Laboratory of High-efficiency Utilization of Coal and Green Chemical Engineering, School of Chemistry and Chemical Engineering, Ningxia University, Yinchuan 750021, China
[c] School of Materials and Chemical Engineering, Xuzhou University of Technology, Xuzhou 221018, China
[d] State Key Laboratory of Coal Conversion, Institute of Coal Chemistry, Chinese Academy of Sciences, Taiyuan 030001, China

ARTICLE INFO

Keywords:
Syngas
Methanol synthesis
Mn promoter
Cu-ZnO_x
Cu and ZnO particle size

ABSTRACT

This study unravels the regulation of Mn promoter in catalytic activity and surface identities of $Cu/ZnO/Al_2O_3$ catalysts by reaction kinetics, TPR/TPD, N_2O titration experiments and in situ spectra techniques. The methanol formation E_A of $Cu/ZnO/Al_2O_3$ catalyst almost remained unchanged with the addition of Mn, confirming the methanol synthesis pathways were not affected. With an increase in the content of Mn, the sizes of Cu and ZnO decreased whereas the reduction degree of ZnO to Zn^0 on the catalyst surface increased, forming more Cu-ZnO_x active sites in CAZ-2%Mn. TPSR confirmed that the amount of the surface CO and H species were highest in CAZ-2%Mn. Therefore, more Cu-ZnO_x active site and surface species in CAZ-2%Mn accounts for the higher methanol formation activity. A detailed understanding of the regulation of Mn in the Cu-ZnO_x sites formation is expected for the precise design of the CuZnAl catalysts for methanol synthesis.

1. Introduction

As a major chemical product and industrial raw material, the global annual output of methanol is more than 100 million tons, and the research of syngas to methanol has attracted attentions worldwide [1,2]. The concept of methanol economy is proposed, the significance of methanol in circular economy has been recognized, and policies have been moved towards the concept of methanol economy in the fuel and chemical industry [3–6]. Currently, the project development of methanol to paraffin and olefin have expanded the methanol market demand [7]. Therefore, the insights into the catalyst design for methanol synthesis play an important role with the rapid development of methanol market and steady increase of output.

$Cu/ZnO/Al_2O_3$ is one of the most widely used catalysts for methanol synthesis. Cu is considered the main active component, ZnO and Al_2O_3 are the support and the promoter of the catalyst respectively [8]. There is a synergistic effect between Cu and ZnO, which can stabilize copper particles and improve their dispersion [9,10]. The formation of excess water can accelerate the crystallization of Cu and ZnO particles in the catalyst, resulting in rapid sintering and deactivation of the catalyst [11]. The addition of the appropriate promoters or supports to Cu/ZnO/Al_2O_3 catalysts is usually to improve the catalytic activity of the catalyst and to clarify the relationship between its structure and activity [12]. The addition of Mg [13], Cr [14] and alkaline earth metal oxides (BaO, CaO and SrO) [15] can improve the specific surface area of the catalyst, increase the dispersion of Cu, generate strong alkaline sites on the surface and promote the adsorption of the syngas. Even though the structure evolution has been extensively investigated, the Cu/ZnO/Al_2O_3 catalysts are still facing the disadvantages of poor hydrothermal stability and unclearly elucidatory structural evolution during the methanol synthesis from syngas.

The active site of the $Cu/ZnO/Al_2O_3$ catalysts is considered Cu surface with the oxygen deficient $Cu_xZn_{(1-x)}O_y$ active phase [10], whereas the metal Cu^0 and partially reduced ZnO_x are proposed active site [16–19], and the catalysis activity is linearly related to the exposure area of copper. The surface of metal Cu is decorated by ZnO_x under relatively

* Corresponding author.
E-mail address: weifengtu@zzu.edu.cn (W. Tu).
[1] The authors with "+" contributed equally to this article.

https://doi.org/10.1016/j.apcatb.2023.122985
Received 27 March 2023; Received in revised form 16 May 2023; Accepted 8 June 2023
Available online 22 June 2023

mild conditions [20], and the reaction energy barrier of methanol synthesis at Cu-ZnO interface is lower than that of CuZn alloy [21]. However, Fujitani and Nakamura obtained completely different conclusions that the active site of the catalyst is composed of ZnO rather than highly dispersed Cu particles [22]. Ostrovskii also reported that ZnO is an active site for methanol synthesis [23]. Although the researches on $CuO/ZnO/Al_2O_3$ catalyst have been deeply studied, the active site of $CuO/ZnO/Al_2O_3$ is still controversial.

Water-gas shift (WGS) reaction occurs simultaneously during the methanol synthesis, which affects the ratio of CO/CO_2 and H_2/H_2O in the reaction atmosphere. It is found that ZnO-free Cu catalyst is inactive for WGS reaction and ZnO plays an important role in WGS [24], whereas the transformation of Zn and ZnO can be regulated by the reduction atmosphere (CO & H_2) [25] and oxidation atmosphere (CO_2 & H_2O) [11]. At the high ratio of CO/CO_2, methanol synthesis activity is strongly interdependent of the Zn coverage [20], whereas the synergy of Cu and ZnO at the interface is considered to facilitate methanol synthesis at low ratio of CO/CO_2 [21]. Therefore, the effect of the WGS on the active sites of $CuO/ZnO/Al_2O_3$ must be controlled in same extent to avoid the controversial conclusions.

Mn is a common promoter in syngas conversion for methanol and higher alcohols synthesis. For higher alcohols synthesis, the interaction between Mn and other metal is considered to regulate the particle size as well as resist the aggregation, apparently affecting the catalysis activity and higher alcohols selectivity [26–28]. The apparent rate constant for CO consumption and the adsorption constant for CO are also affected by the addition of Mn promoter, consequently the moderation of hydrogenation reactions is involved [29,30]. For methanol synthesis. Mn promoter is proposed to decrease Cu particle size and increase the electron-deficient property in CuO, which promotes the methanol productivity and selectivity [31]. Besides, Mn promoted $Cu/ZnO/Al_2O_3$ are investigated in the synthesis of dimethyl ether [32], C_{2+} alcohol [33] and propanoic acid [34], and CuO is confirmed to be easily reduced by the addition of Mn promoters. Even though Mn promoters shows advantages in methanol synthesis and higher alcohols synthesis, little research has focused on the regulation of the Mn promoters on $Cu/ZnO/Al_2O_3$ catalyst for methanol synthesis, and the interaction and structure evolution between Cu and ZnO due to the addition of Mn promoters is still obscure during methanol synthesis.

In this study, we systematically changed the content of Mn promoter in $Cu/ZnO/Al_2O_3$-Mn catalyst to investigate the regulation effect of Mn on the active sites for methanol synthesis from syngas. The catalytic performance of the catalyst was tested by using a fixed bed differential reactor system, and in situ XRD, in situ XPS, in situ DRIFTS, BET, Raman, H_2-TPR, H_2-TPD, CO-TPD, CO_2-TPD, N_2O titration experiments and reaction kinetic analysis were carried out. We demonstrate that the methanol synthesis reaction pathways keep unchanged with the addition of Mn, whereas the sizes of Cu and ZnO decrease and the content of Zn^0 increases, thus forming more Cu-ZnO_x sites in $Cu/ZnO/Al_2O_3$-2%Mn catalyst and improving the TOF of methanol formation. A detailed understanding of the tunable role of Mn in the formation of Cu-ZnO_x sites will be useful for precise design of the CuZnAl catalysts for methanol synthesis.

2. Experiment methods

2.1. Preparation of $Cu/ZnO/Al_2O_3$-Mn catalysts

$Cu/ZnO/Al_2O_3$-Mn catalysts with different Mn contents were prepared by a coprecipitation method. A certain quantity of $Cu(NO_3)_2$ (Macklin, 99.7 % trace metals basis), $Zn(NO_3)_2{\cdot}6\ H_2O$ (Adamas, > 99.0 %), $Al(NO_3)_3{\cdot}9\ H_2O$ (Sinopharm, > 99.0 %) and $C_4H_6MnO_4{\cdot}4\ H_2O$ (Sinopharm, > 99.0 %) were dissolved in 200 mL of double deionized water (> 18.2 MΩ) at room temperature, and the molar ratio was Cu/Zn/Al= 6:3:1 and Mn/Cu = 0.5 %, 1 %, 2 %, 3 %, 4 % and 6 %. A certain stoichiometric quantity of Na_2CO_3 (Macklin, ≥ 99.8 %) (molar ratio, Cu $(NO_3)_2/Na_2CO_3$ = 1, $Zn(NO_3)_2/Na_2CO_3$ = 1 and $Al(NO_3)_3/Na_2CO_3$=2/3) were also dissolved in 200 mL of double deionized water (> 18.2 MΩ) at room temperature. These two solutions were then injected into a beaker containing 300 mL of double deionized water at the same flow rate of 0.74 $mL{\cdot}min^{-1}$ by the peristaltic pumps, and the solution was magnetically stirred at 65 ℃. Then the obtained precipitates were stirred for 1 h and aged for 2 h at 65 ℃, subsequently the precipitate was washed with double deionized water for 15 times. The washed precipitate was dried at 100 ℃ for 12 h, ground into powder and then calcined in a tubular furnace at 350 ℃ for 4 h. The $Cu/ZnO/Al_2O_3$-MnO_2 catalyst was named CZA-xM ($x = n_{Mn}/n_{Cu}$ = 0, 0.5 %, 1 %, 2 %, 3 %, 4 % and 6 %) according to the Mn content. Then the CZA-xM catalyst with particle size range of 120–180 μm was obtained through tablet pressing and screening.

CuO-Mn catalysts with different Mn contents were also prepared by the above method. The CuO–Mn catalyst was named C-xM ($x = n_{Mn}/n_{Cu}$ = 0.5 %, 1 %, 2 %, and 4 %) according to the Mn content. The C-xM catalyst with particle size range of 120–180 μm was obtained through tablet pressing and screening.

2.2. Characterization of catalysts

The number of Cu^0 atoms on the surface was determined by N_2O titration experiment [24,35]. The oxidation process of Cu^0 atom on the catalyst surface was as follows:

$$2Cu + N_2O \rightarrow Cu_2O + N_2 \quad (1)$$

The experiment was carried out by a self-built test device. The reactor was composed of stainless-steel outer tube and quartz inner tube. The gas at the inlet of the reactor was controlled by the mass flowmeters. The K-type thermocouple was inserted from the bottom of the reactor to the bottom of the catalyst bed of the quartz inner tube to monitor the reaction temperature. The gas at the outlet of the reactor was analyzed with the Hidden Analytical quadrupole mass spectrometer. During the test, 100 mg of catalyst (120–180 μm) was pretreated in H_2/Ar (50 $mL{\cdot}min^{-1}$, the volume fraction of H_2 was 5 %) for 3 h, the temperature and pressure were 230 ℃ and 100 kPa. After the reduction process, the H_2/Ar flow was switched to Ar flow and the temperature was decreased to 220 ℃. Then the H_2/Ar flow was switched to the flow of mixture ($H_2/CO/CO_2$ =3:1:0.1, 100 kPa, GHSV=48,000 $mL{\cdot}g_{cat}^{-1}{\cdot}h^{-1}$), and the online analysis of reactants (H_2, CO, CO_2) and product methanol (CH_3OH) was determined by the mass spectrometer at the outlet of the reactor. When the signals of reactants and product were stable, the flow of $H_2/CO/CO_2$ was switched to CO_2/Ar mixture (40 $mL{\cdot}min^{-1}$, CO_2 volume fraction of 5 %) for 0.5 h to oxidize Zn^0 and Mn^{2+} on the catalyst surface, then the CO_2/Ar mixture was switched to Ar (40 $mL{\cdot}min^{-1}$) for purging for 4 h to remove CO_2 in the system, and the system temperature was naturally decreased to 40 ℃. Finally, the Ar flow was switched to N_2O/He mixture (gas flow rate was 20 $mL{\cdot}min^{-1}$ and N_2O volume fraction was 1 %). Meanwhile, the N_2O and N_2 in the outlet gas were analyzed on-line in the whole process by mass spectrometer.

In situ XRD was measured by the D8 advanced X-ray powder diffractometer of Bruker. The radiation source of the instrument was Cu Kα, the scanning range was from 10° to 80°, the scanning step was 0.02° and the scanning rate was $0.033^{\circ}{\cdot}s^{-1}$. Firstly, a flow of 50 $mL{\cdot}min^{-1}$ H_2/Ar mixture was introduced into the sample, the volume ratio of H_2 to Ar was 5:95, the temperature was raised from 30 ℃ to 230 ℃, and spectrums were recorded every 1 h. When the temperature was increased to 230 ℃, the system was remained at this temperature for 8 h, and the spectrums were collected every 2 h. After the reduction treatment, the temperature of the system was decreased to 220 ℃ in the flow of Ar. Then the flow of reaction gas ($H_2/CO/CO_2$ =3:1:0.1, 100 kPa, GHSV=48,000 $mL{\cdot}g_{cat}^{-1}{\cdot}h^{-1}$) was introduced and the spectrums were recorded every 2 h during the reaction process. Based on the full width at half maximum (FWHM) of the characteristic diffraction patterns

measured by XRD experiment, the average particle size was calculated by Scherrer equation [Eq.(2)] as follow :

$$D = \frac{K\gamma}{B\ \cos\theta} \tag{2}$$

Where D is the average thickness of the grain perpendicular to the crystalline facets, K is the Scherrer constant (0.89), γ is the X-ray wavelength (Å), B is the FWHM of the diffraction pattern of the sample and θ is the diffraction angle of the crystalline facets.

In situ XPS experiment was carried out through the in situ XPS system coupled with the self-developed reactor. The reactor was connected to the XPS test chamber through the vacuum pipe. The in situ XPS system was equipped with monochromatic Al-Kα X-ray source (hν = 1486.6 eV) and operated at 15 kV and 80 W. The detector of Phoibos 150 hemispherical analyzer was adopted. The XPS test chamber was equipped with a laser heater, which could heat the catalyst to the temperature required for the reaction. The vacuum degree of the system could reach 10^{-10} mbar. The measured XPS spectra were calibrated according to the C 1 s binding energy (284.8 eV). The catalyst power was pressed into the stainless-steel mesh, transferred into the reactor, subsequently pretreated in H_2/Ar (50 mL·min^{-1}, the volume fraction of H_2 was 5 %) at 500 kPa and 230 ℃ for 3 h, then the temperature was decreased to 220 ℃ in the flow of Ar. After the reduction process, the catalyst was exposed to H_2-CO-CO_2 mixture (1500 kPa, the volume ratio is 3/1/0.1, GHSV = 48,000 mL·g_{cat}^{-1}·h^{-1}) for 3 h. After the reaction process, the sample was transferred into the XPS test chamber. During sample pretreatment, the vacuum pipe was opened through two gate valves to ensure that the vacuum pipe system was in a vacuum environment during sample transfer. After the sample had been moved into the XPS test chamber, the reaction was continued at 220 ℃ in the mixture of H_2-CO-CO_2, and the in situ XPS data was recorded simultaneously.

In situ DRIFTS experiment was measured by Thermo iS50 of Harrick Scientific company. The instrument had a high temperature reaction chamber equipped with ZnSe window and an intelligent MCT liquid nitrogen cooling detector. The resolution was 4 cm^{-1} and the scanning range was from 1000 cm^{-1} to 4000 cm^{-1}. The catalyst powder was pretreated in H_2/Ar (50 mL·min^{-1}, the volume fraction of H_2 was 5 %) at 230 ℃ and 100 kPa for 3 h. After the reduction process, the reaction flow was switched to Ar (40 mL·min^{-1}) and the catalyst was purged for 4 h, and the reaction temperature was naturally decreased to 40 ℃, then the background was collected at 40 ℃. Subsequently, Switched Ar flow to CO/Ar mixture (40 mL·min^{-1}, 5 % CO volume fraction) for 0.5 h, then switched back to Ar (40 mL·min^{-1}) again for purging for 0.5 h, and infrared spectras were collected during adsorption and purging respectively.

2.3. Steady-state catalytic rate

The catalysis performance and kinetics were tested in a fixed bed differential reactor system. The reactor consisted of stainless-steel outer tube (total length 400 mm) and quartz inner tube (4.0 mm diameter). The stainless-steel outer tube was heated by an external program-controlled tubular furnace (Hangzhou Zhuochi Instrument Co., Ltd., 30165–10 M). The reaction temperature was controlled by the temperature control cabinet (Xiamen Yudian Automation Technology Co., Ltd., 716 P) and the K-type thermocouple was inserted from the bottom of the reactor to the bottom of the catalyst bed of the quartz inner tube to monitor the reaction temperature. The reaction gas was controlled by four gas mass flowmeters (Brooks Instrument, SLA5800). The reaction pressure was controlled by TESCOM26–1765 back pressure valve installed at the outlet of the reactor, and the precision pressure sensor (MKS , 750C12PFF2GA) was installed at the inlet of the reactor to monitor the reaction pressure. The on-line gas chromatograph (Shanghai Ruimin Instrument Co., Ltd., GC2060) was used for on-line analysis of the outlet gas of the reactor. The gas chromatograph was equipped with H_2 Flame ion detector (FID) connected with capillary chromatographic column (Agilent, HP-PLOT-Q), methane reformer and FID detector connected in series with Porapak-Q chromatographic column, and thermal conductivity detector (TCD) connected with TDX-01 packed chromatographic column. Before the test, 100 mg of catalyst (120–180 μm) was put into the quartz inner tube, and the catalyst was fixed with quartz cotton to ensure that the catalyst was in the constant temperature zone of the reactor.

The catalyst was pretreated in H_2/Ar (50 mL·min^{-1}, the volume fraction of H_2 was 5 %) for 3 h, the temperature and pressure were 230 ℃ and 500 kPa. Then the pressure was increased to 1500 kPa and the temperature was decreased to 220 ℃ in the flow of Ar. Finally, the catalyst was exposure to H_2-CO-CO_2 mixture (1500 kPa, the volume ratio is 3/1/0.1, GHSV = 48,000 mL·g_{cat}^{-1}·h^{-1}). The formation rate of CH_3OH was the molar amount of CH_3OH generated on the catalyst per unit mass per unit time [Eq.(3)]:

$$r_{CH_3OH}/(mol\cdot g_{cat}{}^{-1}\cdot s^{-1}) = \frac{n^{out}_{CH_3OH}}{m_{cat}} \tag{3}$$

Where $n^{out}_{CH_3OH}$ is the molar amount of CH_3OH at the outlet of the reactor in unit time (mol·s^{-1}), m_{cat} is the mass of catalyst (g).

Methanol selectivity refers to the ratio of methanol to the total amount of consumed CO and CO_2, as shown in Eq.(4) :

$$S_{CH_3OH}/(\%) = \frac{n^{out}_{CH_3OH}}{n^{in}_{CO} - n^{out}_{CO} + n^{in}_{CO_2} - n^{out}_{CO_2}} \tag{4}$$

Where n_i^{in} is the molar amount of CO or CO_2 at the inlet of the reactor in unit time (mol·s^{-1}), n_i^{out} is the molar amount of CO, CO_2 or CH_3OH at the outlet of the reactor in unit time (mol·s^{-1}).

The turnover frequency (TOF) refers to the ratio between the positive reaction rate and the number of surface Cu^0 sites unit mass catalyst calculated by N_2O titration experiment [Eq. (5)]:

$$TOF_{CH_3OH}/(s^{-1}) = \frac{r_{CH_3OH}}{n_{cu^0}} \tag{5}$$

Where n_{cu^0} is the number of metal Cu^0 atoms on the surface of catalyst per unit mass (mol·g^{-1}).

The apparent activation energy of the catalyst was measured as follows. The catalyst was pretreated in H_2/Ar (50 mL·min^{-1}, the volume fraction of H_2 was 5%) 230 ℃ and 500 kPa for 3 h. After the pretreatment process, the temperature was decreased down to 190 ℃ in the flow of Ar and the pressure was increased to 1500 kPa, and the catalyst was exposed to the reaction gas. The reaction temperature was continuously increased to 200 ℃, 210 ℃, 220 ℃ and 230 ℃. At each reaction temperature, the reaction lasted enough time to ensure that the catalyst was a stable state. Then the reaction temperature was decreased to 190 ℃ at the end to ensure that there was no deactivation during the reaction.

The water-gas-shift (WGS) reaction and methanol synthesis reaction occurred simultaneously. η_{WGS} referred to the approach degree of WGS reaction from chemical equilibrium during methanol synthesis reaction [Eq. (6)]. In the equation, the partial pressure of H_2O was determined by the balance of oxygen atoms in reactants and products, ignoring other oxygenated substances generated by CO_2 hydrogenation (The selectivity of oxygenated substances is less than 1.0% under all test conditions).

$$\eta_{WGS} = \frac{P_{CO_2}P_{H_2}}{P_{CO}P_{H_2O}} \times \frac{1}{K_{eq,WGS}} \tag{6}$$

Where P_i is the partial pressure of each substance (CO, H_2O, CO_2 and H_2) at the outlet of the reactor, $K_{eq,WGS}$ is the equilibrium constant of WGS reaction.

The conversion rate of CO was lower than 5 % during the catalysis activity test and catalyst kinetics test, the purpose of which was to

ensure that the real methanol synthesis rate could be measured under different reaction conditions. The detailed information of BET, Raman, H_2-TPR, H_2-TPD, CO-TPD and CO_2-TPD are shown in Supporting information materials.

3. Result and discussion

3.1. Crystalline structure and surface area the fresh calcined catalyst

The BET surface area of the fresh CZA-xMn catalyst is shown in Table S1. With an increase in Mn content, the specific surface area of CZA-xMn catalyst firstly increased and then deceased, and the CZA-2% Mn had the maxmium specific surface area. In Fig. 1a, the diffraction patterns at 35.5° and 38.7° corresponded to (002) and (111) crystal planes of CuO (PDF#45–0937), the diffraction patterns at 31.8° and 36.3° corresponded to (100) and (101) crystal planes of ZnO (PDF#36–1451). The XRD patterns of MnO_2 were not be detected, which was probably due to the high dispersion of manganese oxide. The particle size of CuO calculated by the Scherrer equation is shown in Table S2, whereas the size of ZnO could not be calculated exactly due to the weak diffraction patterns. With an increase in content of Mn, the particle size of CuO slightly decreased from 6.0 nm to 5.0 nm. Besides, the elemental mapping of CZA-2%Mn in Fig. 2a-f showed the elements (Cu, Ce, Al, Mn, O) were uniformly distributed on the catalyst, and TEM images of CZA-2%Mn catalyst in Fig. 2g-h further confirmed that the CuO nanoparticle were contact with the ZnO nanoparticle. In Fig. 1b, the peaks at 600 cm^{-1} and 1100 cm^{-1} in the Raman spectra were related to the oxygen vacancy of the catalyst [36,37], and that of CZA-2%Mn catalyst was higher than other CZA-xMn catalysts.

3.2. Catalyst structure evolution during the reaction

The XRD patterns of CZA-xMn after reduction for 6 h are shown in Fig. 3a, and the XRD patterns of the reduced CZA-xMn after subsequent reaction for 6 h are shown in Fig. 3b. Compared with the XRD patterns of the fresh catalyst in Fig. 1a, the diffraction patterns of CuO at 35.5° and 38.7° disappeared and were replaced by two characteristic diffraction patterns of metal Cu^0 at 43.3° and 50.4° in Fig. 3. The weak characteristic diffraction patterns of ZnO at 31.8°, 34.4°, 36.2°, 56.6°, 62.9° and 66.4° were observed, and the weak diffraction patterns of MnO_2 at 56.0° were detected in CZA-2%Mn and CZA-4%Mn. Therefore, CuO in the catalyst was reduced to metal Cu^0 and Zn species was mainly in the form of ZnO after the reduction process for 6 h. Besides, the XRD pattern of the reduced CZA-x%Mn catalysts during the subsequent reaction (2–10 h) are shown in Fig. 4 and S1. During the reaction from 2 h to 10 h, the diffraction patterns of Cu^0 and ZnO almost remained unchanged, and the diffraction patterns of new species were not detected with the increase of reaction time, indicating the crystalline size of the Cu^0 and ZnO remained unchanged during the reaction.

Based on the diffraction patterns in Fig. 3, the crystalline size of Cu^0 and ZnO calculated by Scherrer equation are shown in Table 1. For the catalyst of CZA, the crystalline size calculated by Cu (200) was 4.6 nm in Fig. 3a, whereas that calculated by Cu (200) increased to 6.1 nm in Fig. 3b, and the size calculated by ZnO (100) also increased from 5.1 nm to 7.9 nm. However, the crystalline size of Cu and ZnO species in Fig. 3a were almost unchanged compared to that of Cu and ZnO species in Fig. 3b with the addition of Mn from 0.5 % to 4.0 %, especially for the size calculated by Cu (200) and ZnO (100). Therefore, the aggregation of Cu and ZnO species from the reduction process to reaction process were inhibited by the Mn addition.

When the reduced CZA-x%Mn underwent the subsequent reaction for 6 h, the crystalline size of Cu and ZnO in Fig. 3b firstly decreased and then increased with the increasing content of Mn from 0 % to 4.0 %, and the smaller size of Cu and ZnO was obtained in CZA-2%Mn. This phenomenon is probably due to the addition of Mn promoted the dispersion of Cu and ZnO, whereas the promotion effect was inhibited by the addition of excessive Mn.

3.3. Catalyst valence states evolution and CO adsorption sites during the reaction

The valence states of CZA-xMn catalyst were analyzed by in situ XPS, and the contents of surface species during the reaction are shown in Table 2. The mole ratio of Cu/Zn/Al in CZA-xMn catalyst was close to 6/3/1, which was consistent with the content of CZA-xMn catalyst in the preparation procedure. When the Mn content was less than 4 %, the binding energy peaks of Mn was too weak to exactly calculate the ratio of Mn to the surface atoms.

In Fig. 5a, the peaks at 951.9 eV and 932.2 eV were attributed to the binding energy (BE) of Cu $2p_{1/2}$ and Cu $2p_{3/2}$ and no obvious satellite peaks of Cu^{2+} were observed in the range of 940–942.5 eV, indicating that Cu species on the surface of catalyst exists in the form of reduced state (Cu^+ or Cu^0) during the reaction. The BE of Cu^+ and Cu^0 2p spectra are at 932 eV [38–41], whereas no satellite peaks of Cu^+ were observed in the range of 941–949 eV. The kinetic energy (KE) difference between Cu^+ and Cu^0 in Cu Auger LMM spectra is about 2 eV (916.8 eV for Cu^+ and 918.6 eV for Cu^0) [42]. In Fig. 5b, the KE of Cu LMM of CZA-xMn catalysts are at 919.1 eV, further indicating that CuO had been completely reduced to metal Cu^0 atom during the reaction.

In Fig. 5c, the BE peaks at 1021.6 eV were mainly attributed to ZnO [43]. In Fig. 5d, it was found that there was a small amount of metal Zn^0 on the surface of the catalyst through the fitting of Zn Auger LMM spectra, indicating that ZnO in the catalyst had been partially reduced to Zn^0 during reduction and reaction [44]. The ratio of the peak area of

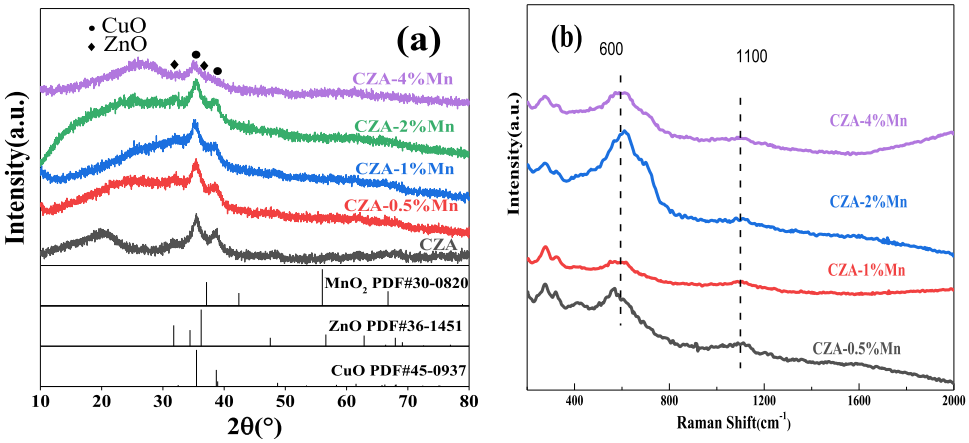

Fig. 1. (a) XRD patterns and (b) Raman spectra of the fresh CZA-xMn catalysts.

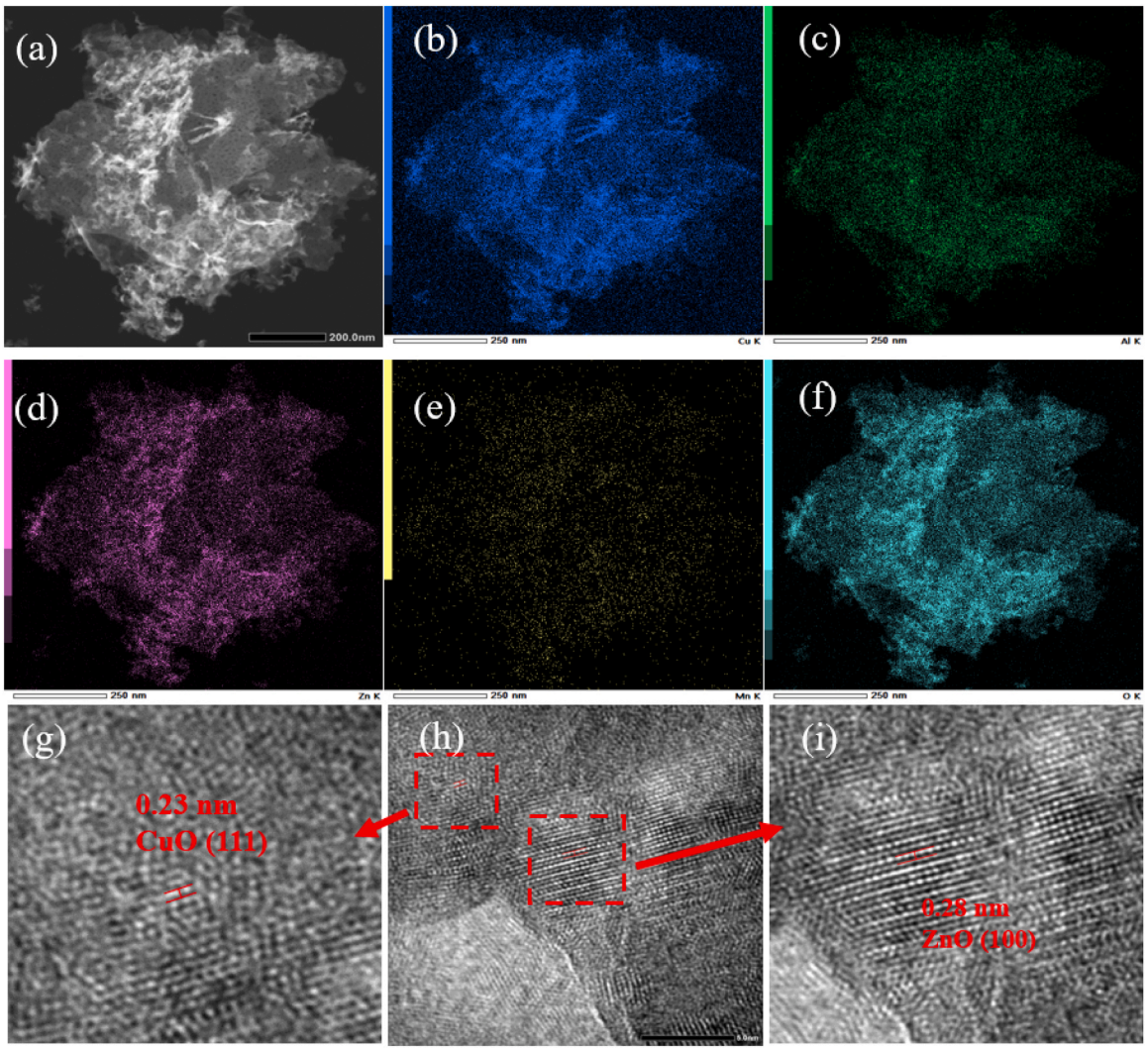

Fig. 2. (a–d) The elemental mapping of CZA-2%Mn catalyst. Cu (b), Al (c), Zn (d), Mn (e), O (f), Scale bar: (a) 200 nm (b-f) 250 nm. (g-i) TEM images of CZA-2%Mn catalyst, Scale bar:5 nm.

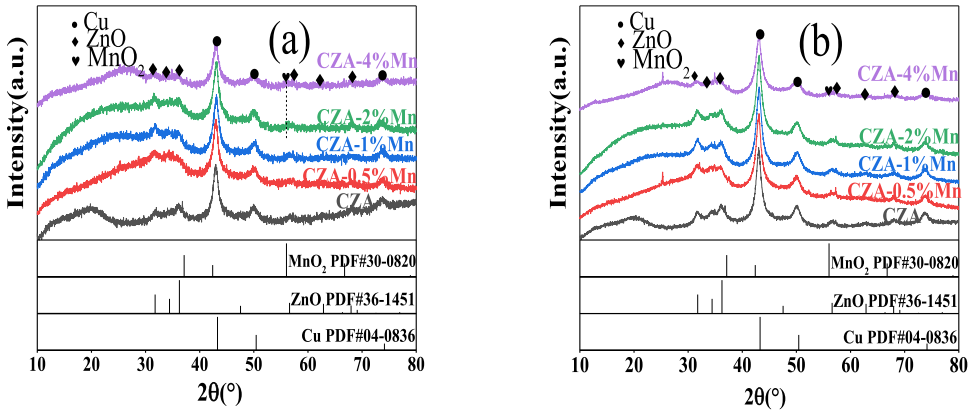

Fig. 3. XRD patterns of CZA-xMn catalyst (a) after reduction for 6 h and (b) subsequent reaction for 6 h.

metal Zn^0 and ZnO to the area of Zn LMM (Zn^0/Zn, Zn^{2+}/Zn) during the reaction process is shown in Table 3. With the increasing content of Mn from 0% to 2%, the content of metal Zn^0 increased gradually from 12.4% to 21.5%, indicating the addition of Mn promoted the reduction of ZnO. However, the content of metal Zn^0 decreased from 21.5% to 14.5% with the increasing content of Mn from 2 % to 4 %, which was probably due to that the addition of excessive Mn inhibited the reduction of ZnO to metal Zn^0.

In Fig. 6a, O 1 s XPS curves of CZA-xMn catalysts during the reaction showed three peaks (α, β and γ), which were attributed to surface hydroxyl group, surface oxygen O_{ads} (O^-, O_2^- or O_2^{2-}) and lattice oxygen O_{latt} (O^{2-}) species, respectively [45]. O_{ads} (Peak β) was related to the oxygen

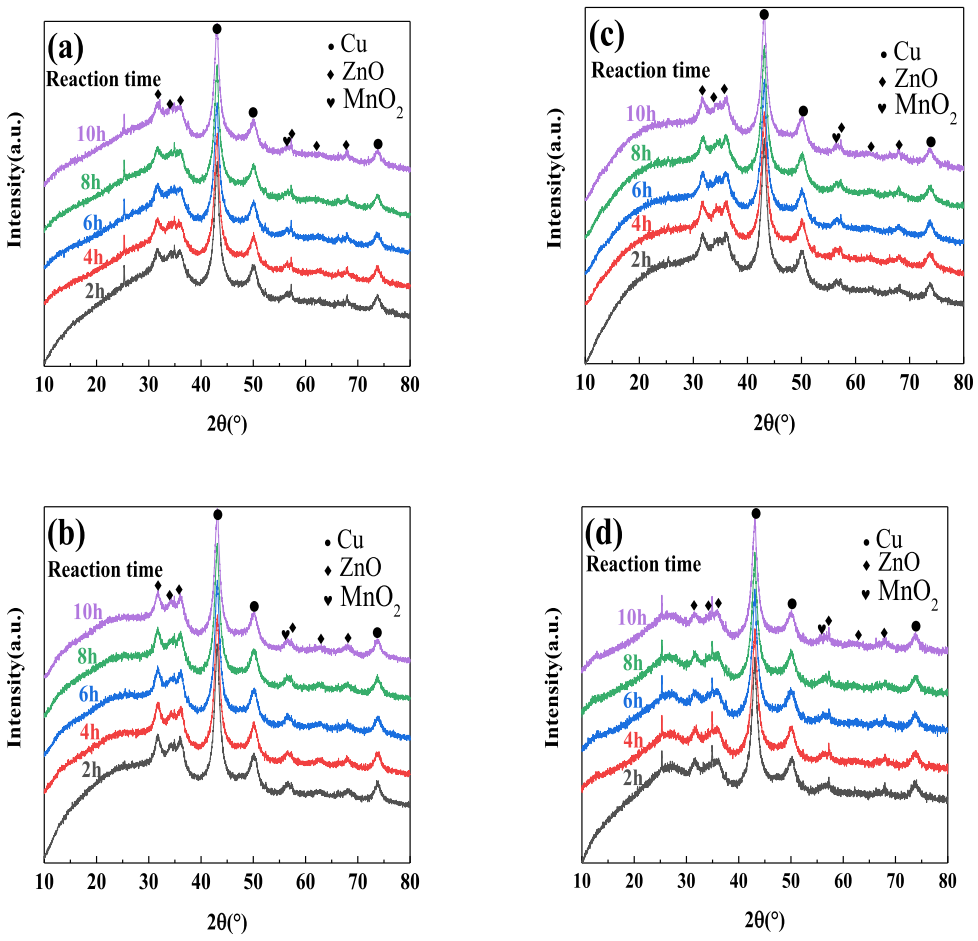

Fig. 4. XRD patterns of (a) CZA-0.5%Mn; (b) CZA-1%Mn; (c) CZA-2%Mn; (d) CZA-4%Mn catalysts during the reaction.

Table 1
Crystalline size of Cu and ZnO in the CZA-xMn catalysts after reduction for 6 h and subsequent reaction for 6 h.

Samples	Reduction for 6 h (nm)			Subsequent reaction for 6 h (nm)		
	Cu (111)	Cu (200)	ZnO (100)	Cu (111)	Cu (200)	ZnO (100)
CZA	7.1	4.6	5.1	7.7	6.1	7.9
CZA-0.5%Mn	6.9	5.5	7.1	7.0	5.4	7.3
CZA-1%Mn	6.8	5.7	6.3	6.7	5.5	6.0
CZA-2%Mn	6.3	5.6	5.9	6.7	5.4	6.1
CZA-4%Mn	7.3	6.0	6.0	7.1	5.9	6.3

Table 2
Contents of different species on the surface of CZA-xMn catalysts during the reaction.

Sample	Cu/ (Cu+Zn+Al+Mn)[a] (%)	Zn/ (Cu+Zn+Al+Mn)[a] (%)	Al/ (Cu+Zn+Al+Mn)[a] (%)	Mn/ (Cu+Zn+ Al+Mn)[a] (%)
CZA-0.5%Mn	59.1	31.2	9.7	—
CZA-1%Mn	57.1	32.2	10.7	—
CZA-2%Mn	59.8	29.8	10.4	—
CZA-4%Mn	60.8	27.6	9.7	1.9

[a] The atomic ratio.

vacancy on the catalyst surface [46]. Surface oxygen atomic area ratio are shown in Table 4. With the increasing content of Mn promoters, the number of oxygen vacancies on the catalyst surface first increased and then decreased. The formation of metal Zn^0 increased the number of oxygen vacancies in ZnO_x, and the highest content of oxygen vacancies was obtained in CZA-2%Mn. In situ DRIFTS are shown in Fig. 6b. The peaks at 2097 cm^{-1} were assigned to the infrared vibration peak of CO on Cu^0 site [47]. The infrared vibration peak of CO adsorption on Cu^0 site was not detected in the CuO catalyst under the same test conditions, whereas the infrared vibration peak of CO adsorption on Cu^0 site could be detected in the CZA catalysts. Therefore, the adsorption site of CO was on the Cu-ZnO site rather than the single Cu^0 site on the catalyst surface.

The XPS showed that ZnO on the catalyst surface had been partially reduced to metal Zn^0 during the reaction, and the metal Zn^0 content in ZnO_x was the highest when Mn content was 2%. The partially reduced ZnO could form Cu-ZnO_x site [48,49], which was due to the Support-Metal Strong Interaction [50,51] and the difference of surface

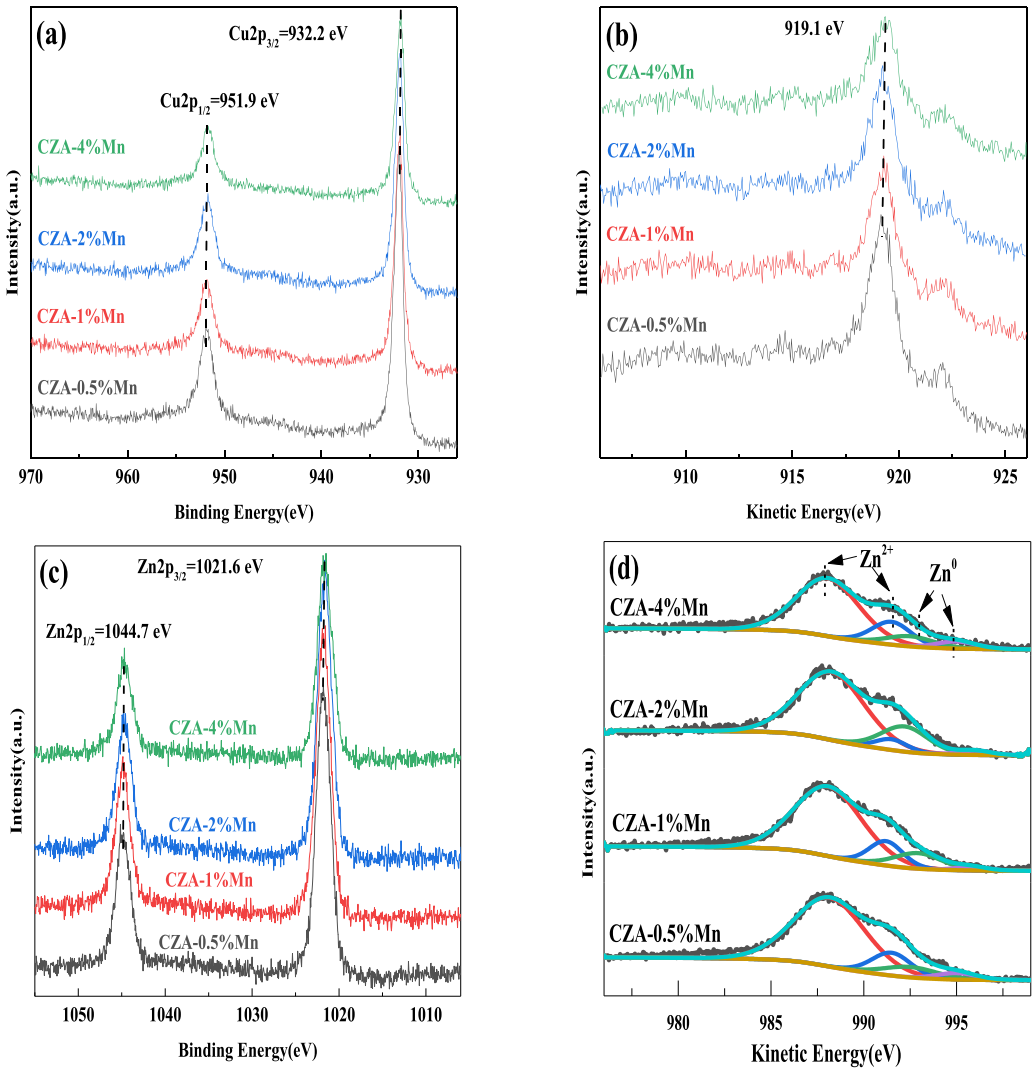

Fig. 5. In situ XPS of (a) Cu 2p, (b) Cu LMM, (c) Zn 2p and (d) Zn LMM on the CZA-xMn surface during the reaction.

Table 3
The content of Zn^0 and Zn^{2+} on the surface of the CZA-xMn catalyst during the reaction.

Sample	Cu $2p_{3/2}$ (eV)	Zn $2p_{3/2}$ (eV)	Zn^0/Zn (%)[a]	Zn^{2+}/Zn (%)[a]
CZA-0.5%Mn	932.1	1021.8	12.4	87.6
CZA-1%Mn	931.9	1021.8	13.3	86.7
CZA-2%Mn	932.3	1021.8	21.5	78.5
CZA-4%Mn	932.2	1021.6	14.5	85.5

[a] peak area ratio.

free energy between Cu and ZnO [52]. In Fig. 6b, the adsorption strength of CO gradually increased and then decreased with the increase of Mn content, and the maximum value was obtained in the CZA-2%Mn. Besides, Fig. S2 and Table S3 confirmed the highest content of Mn^{2+} was obtained over CZA-2%Mn. Therefore, the adsorption site of CO was further identified as the Cu-ZnO_x sites regulated by Mn promoters during the reaction.

3.4. H_2-TPR of the fresh calcined CZA-xMn catalysts and (H_2, CO and CO_2)-TPD of the CZA-xMn catalysts after the reaction

In Fig. 7a, the reduction peaks of the fresh calcined CZA-xMn catalyst at 180–280 ℃ were attributed to the reduction of CuO to Cu [53], which was consistent with the XRD patterns. In Fig. 7b, the peaks α, β and γ at the lower temperature were assigned to the molecular H_2 and free H atom on the catalyst surface, whereas the peak δ at the higher temperature belonged to the H atom on the surface of Cu-ZnO_x [54–56]. The area ratio variation of δ with Mn content is shown in Table S4. CO-TPD curve of the spent CZA-xMn catalyst is shown in Fig. 7c and the ratio of the peaks is shown in Table S5. The desorption peaks concluded three peaks (α, β, γ) at 70–270 ℃. Peak α was attributed to weakly adsorbed CO on the catalyst surface, peak β and peak γ were strongly adsorbed CO at the Cu site on the catalyst surface. The CO_2-TPD of the spent CZA-xMn catalyst are shown in Fig. 7d. The weak basic sites (α) were related to surface OH^-, the medium basic sites (β) were related to metal-oxygen pairs, and the strong basic sites (γ) were related to low coordinated oxygen anions [57]. With an increase in the content of Mn, the surface H atom and the adsorption capacity of CO increased firstly and then decreased, and the adsorption capacity of H atom and CO reached the maximum on the surface of CZA-2%Mn catalyst.

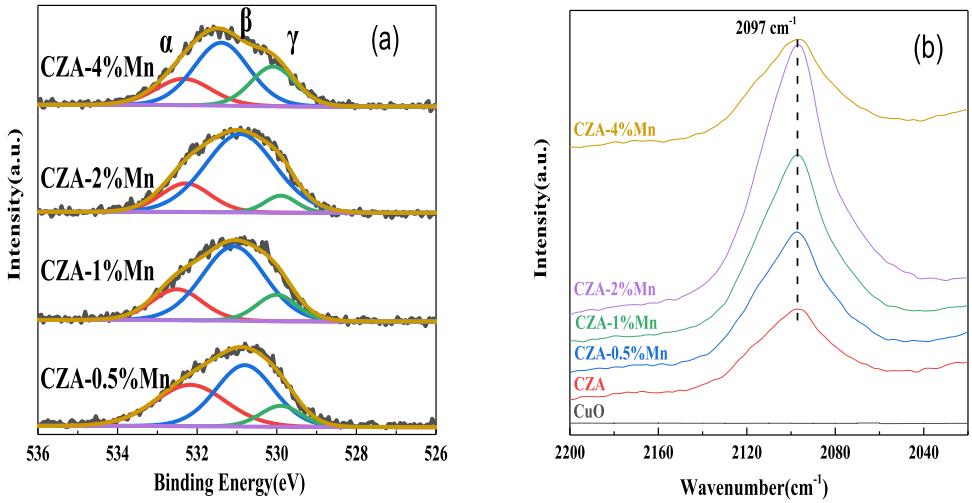

Fig. 6. In situ XPS of (a) O 1 s and in situ DRIFTS (b) of CZA-xMn catalysts during the reaction.

Table 4
Surface oxygen atomic concentration and area ratio data from XPS analysis for CZA-xMn catalysts.

Samples	Total surface oxygen concentration (%)	Surface oxygen atomic area ratio (%)		
		α	β	γ
CZA-0.5%Mn	34.6	37.8	48.5	13.7
CZA-1%Mn	35.1	21.3	64.1	14.6
CZA-2%Mn	34.9	19.0	73.7	7.3
CZA-4%Mn	35.1	21.8	51.8	26.4

3.5. The titration experiment of Cu^0 and Zn^0 on the surface of spent CZA-xMn and the Mn^{2+} content on the surface of spent C-xMn

The N_2O titration experiment curves of spent CZA-xMn catalysts are shown in Fig. S3. There were a variety of reduced metal species (Cu^0, Zn^0 and Mn^{2+}) in the reaction process. Therefore, the number of surface reduced metal species was named n_{All} and shown in Fig. 8a. The n_{All} first increased and then decreased with the increasing content of Mn. When the Mn content was 2 %, the highest content of n_{All} reached 7.7×10^{-4} mol·g_{cat}^{-1}. The atomic number of Cu^0 on the surface of spent CZA-xMn catalyst after CO_2 treatment determined through N_2O titration experiment are shown in Fig. S4. The N_2O adsorption capacity of CZA-xMn catalyst after CO_2 treatment significantly decreased compared to that without CO_2 treatment in Fig. S3, which was due to that the reduced metal species (Zn^0, Mn^{2+}) on the catalyst surface were oxidized by CO_2 and only the metal Cu^0 was left on the catalyst surface. Therefore, the number of Cu^0 atoms on the spent CZA-xMn catalyst can be calculated by Fig. S4 and shown in Fig. 8b. The number of Cu^0 atoms on the surface of spent CZA-xMn catalyst basically maintained at 5.5×10^{-4} mol·g_{cat}^{-1}.

The number of reduced metal species (Cu^0, Zn^0 and Mn^{2+}) on the surface of the spent CZA-xMn without CO_2 treatment can be described as A, the number of the metal Cu^0 atom on the spent CZA-xMn surface after CO_2 treatment can be described as B, therefore, the difference between them (A-B) was the sum of the number of Zn^0 and Mn^{2+} on the catalyst surface (recorded as $n_{Zn,Mn}^{0,2+}$), and $n_{Zn,Mn}^{0,2+}$ content variation with the Mn content is shown in Fig. 8c. In order to calculate Zn^0 and Mn^{2+} content on the surface respectively, N_2O titration experiments on the spent C-xMn catalysts with CO_2 treatment and without CO_2 treatment were carried out and shown in Fig. 9. The adsorption capacity of N_2O on C-xMn catalyst changed significantly with CO_2 treatment and without CO_2 treatment. Since the weak oxidation of CO_2 had no effect on Cu^0 on the catalyst surface, it further confirmed that CO_2 could oxidize Mn^{2+} on the catalyst surface, and Mn^{2+} content is shown in Fig. 8d. According to Fig. 8c and d, the proportion of Mn^{2+} content in the total content of Zn^0 and Mn^{2+} is below 0.1 for CZA-0.5%Mn, CZA-1%Mn and CZA-2%Mn. Therefore, $n_{Zn,Mn}^{0,2+}$ is approximately the number of Zn^0 atoms on the surface. Trend in Fig. 8c increased first and then decreased, and its content reached the maximum CZA-2%Mn, which further showed that the addition of Mn promoted more ZnO reduction to metal Zn^0, thus promoting the formation of Cu-ZnO_x sites on the catalyst surface.

3.6. Catalytic performance and reaction kinetic analysis

The methanol formation rates of CZA-xMn catalyst and C-xMn catalyst are shown in Fig. 10a. The methanol formation rate on Cu/ZnO/Al_2O_3 catalyst without Mn was only 3.4×10^{-6} mol·g_{cat}^{-1}·s^{-1}. With the increase of Mn content, the methanol formation rate on the CZA-xMn catalyst first increased and then decreased. When the Mn content was 2%, the maximum methanol formation rate on the catalyst was 6.4×10^{-6} mol·g_{cat}^{-1}·s^{-1}. It showed that the addition of an appropriate amount of Mn improved the methanol formation rate on the catalyst. Besides, C-xMn catalyst almost had no methanol synthesis activity, and Mn content had no effect on the methanol formation rate of C-xMn catalyst. Therefore, the higher methanol formation rate of CZA-xMn catalyst was mainly attributed to the interaction between Cu and Zn species, which was consistent with conclusion that the active site of Cu-ZnO catalyst was related to the synergy between partially or completely reduced Cu and ZnO or partially reduced ZnO_x [10,58,59]. The TOF of CZA-xMn catalysts was calculated based on the number of Cu^0 atoms on the catalyst surface and shown in Fig. 10b. The TOF of Cu/ZnO/Al_2O_3 catalyst was only 6.1×10^{-3} s^{-1}, whereas the methanol synthesis activity of the catalyst firstly increased and then decreased with the increasing content of Mn. When the Mn content was 2%, the highest TOF was 1.2×10^{-2} s^{-1}. Therefore, the TOF and methanol formation rate of CZA-xMn catalyst first increased and then decreased, and reached the maximum value when the Mn content was 2 %. In situ XRD, in situ XPS and in situ DRIFTS showed the content of metal Zn^0 and oxygen vacancy in the spent CZA-xMn catalyst were highest in CZA-2%Mn, consequently

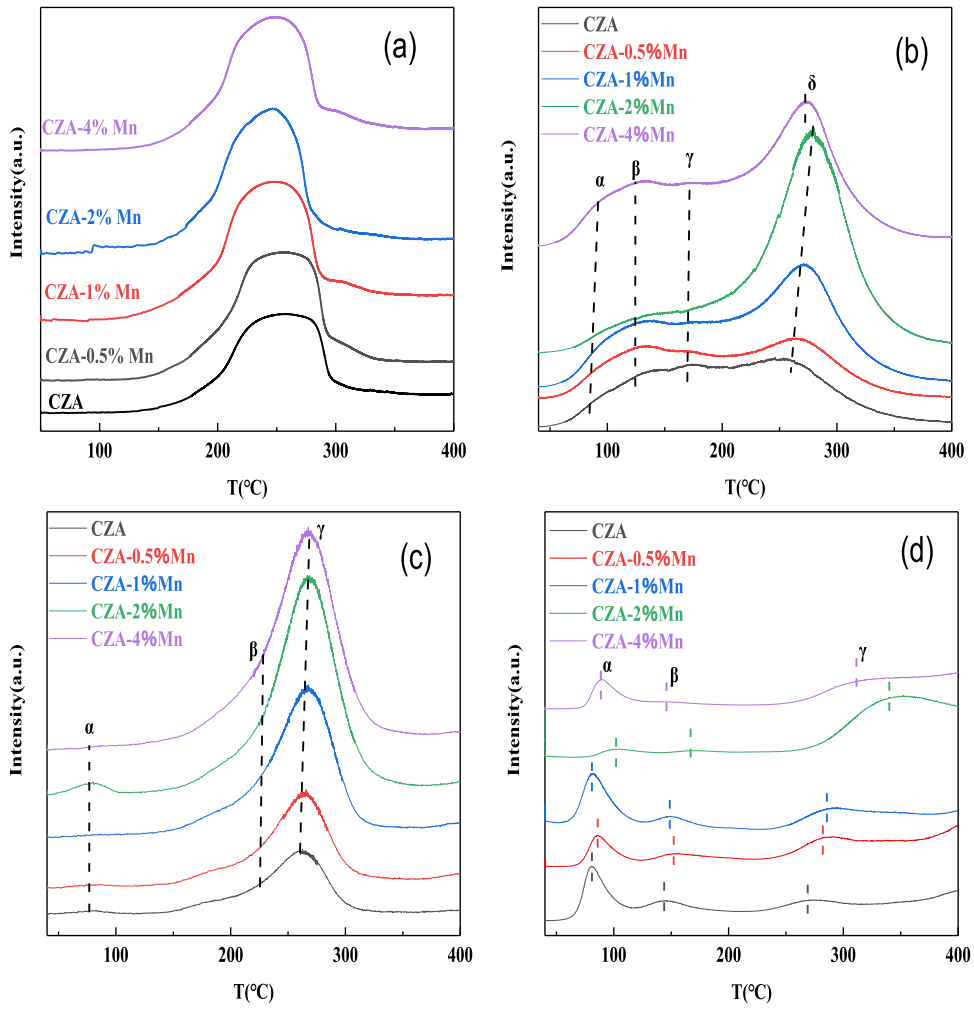

Fig. 7. H_2-TPR curves (a) of the fresh calcined CZA-xMn catalysts, H_2-TPD (b), CO-TPD (c) and CO_2-TPD curves (d) of the spent CZA-xMn catalysts.

the highest content of Cu-ZnO_x interfaces was obtained. Therefore, the highest TOF and methanol formation rate were associated with the most Cu-ZnO_x interfaces in the catalyst of CZA-2%Mn.

The methanol selectivity and formation rate variation with the reaction time are shown in Fig. 11a. The methanol formation rate remained unchanged at 2.3×10^{-4} mol·g^{-1}·s^{-1} and the selectivity of methanol was higher than 95 % during the reaction, which showed that CZA-2%Mn had a good stability. Water-Gas Shift (WGS) reaction and methanol synthesis reaction occurred simultaneously. The formation of excessive water was proposed to accelerate the crystallization of Cu and ZnO particles in the catalyst and result in rapid sintering and deactivation of the catalyst [11]. In order to judge the effect of WGS reaction on methanol synthesis reaction, the constant of WGS reaction close to chemical equilibrium (η_{WGS}) was shown in Fig. 11b. The η_{WGS} of CZA-xMn catalyst did not change with the change of Mn content, indicating that the degree of WGS reaction on different catalysts was the same and its impact on the Cu and ZnO particles and methanol synthesis reaction was negligible.

Fig. 11c and d show the TOF variation trend with temperature and CZA-xMn catalyst apparent activation energy (E_A) variation trend with different Mn content. From the slope of the straight line in Fig. 11c, the E_A of methanol formation of CZA-xMn catalyst could be deduced and shown in Fig. 11d. The E_A of methanol formation of CZA-xMn catalyst was 77–81 kJ·mol^{-1}, which was consistent with the data of Cu/SiO_2 catalyst (88 kJ·mol^{-1}) reported by Clarke et al. [60] and polycrystalline copper catalyst (77 kJ·mol^{-1}) reported by Campbell et al. [61]. The E_A of methanol formation of CZA-xMn almost kept unchanged with the increase of Mn content, indicating that the reaction pathways or the adsorption energy of intermediate products [62] maintained unchanged with the addition of Mn whereas the methanol synthesis activity of the catalyst was regulated by the number of Cu-ZnO_x interface sites.

3.7. *The mechanism of methanol synthesis in the CZA-xMn catalysts*

The methanol synthesis pathways are discussed according to the kinetics reaction results. The E_A of methanol formation of CZA-xMn remained unchanged with the increase content of Mn, and the value of E_A was consistent with the literatures [60,61], which indicated that the reaction pathway or the adsorption energy of intermediate products kept unchanged with the addition of Mn. Therefore, the number of active sites and the surface species are discussed below, and the regulation of Mn in Cu-ZnO_x formation during methanol synthesis from syngas over $Cu/ZnO/Al_2O_3$-MnO_2 catalysts is shown in Scheme 1.

ZnO could not be reduced by H_2 in the reaction conditions [21], whereas the contact between Cu and ZnO favored the electronic transfer from ZnO to Cu and the formation of the oxygen vacancies in ZnO, thus forming Cu-ZnO_x sites [10]. In situ XPS in Fig. 5 and S2 showed little percent of O in ZnO was removed during the reaction, resulting in the formation of little Zn^0 in ZnO_x. The framework of ZnO_x is still ZnO in spite of the formation of Zn^0. Therefore, the form of ZnO_x in Cu-ZnO_x

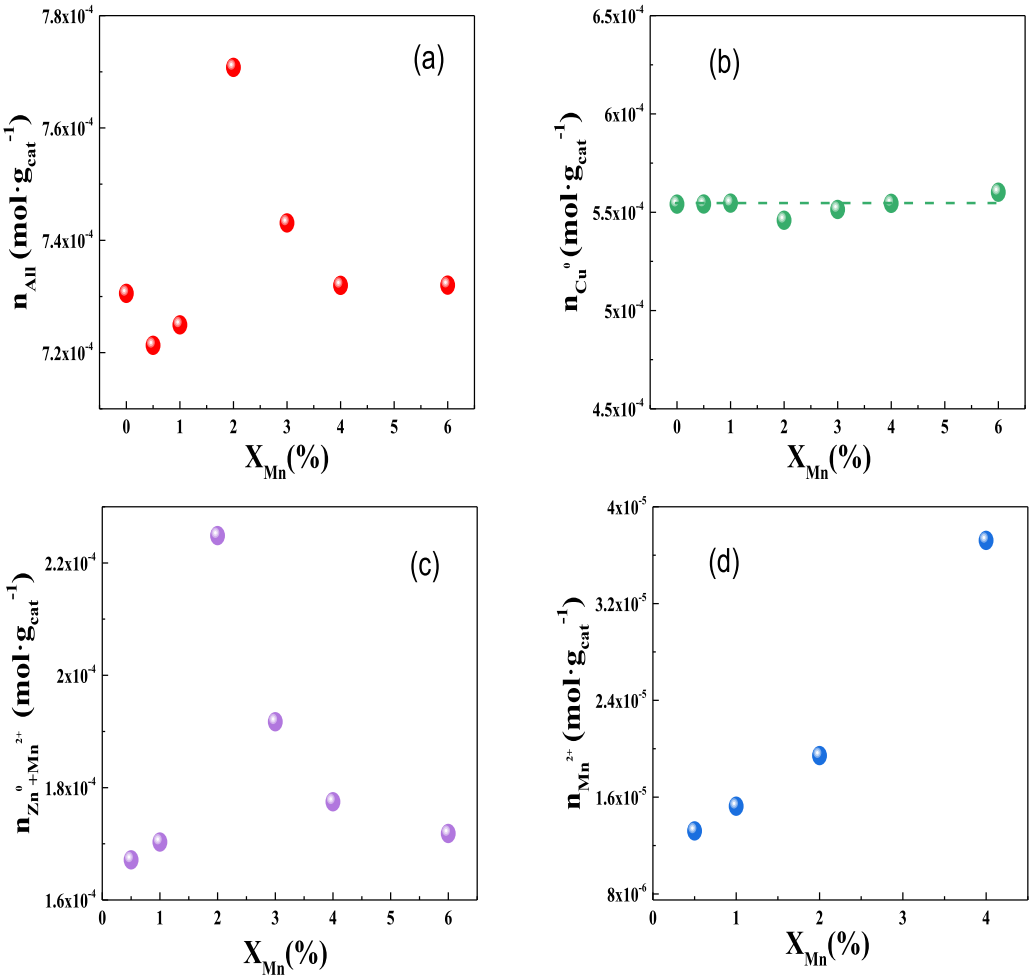

Fig. 8. Number of surface reduced metal species atoms (a), Cu^0 atoms (b), Zn^0 and Mn^{2+} content (c) on the surface of CZA-xMn catalysts during the reaction, and Mn^{2+} content on surface of C-xMn catalysts during the reaction (d).

mainly consists of ZnO and partially reduced ZnO. In this work, the active sites of the CZA-xMn catalyst for methanol synthesis are considered Cu-ZnO_x sites.

The regulation of Mn in the number of Cu-ZnO_x sites can be discussed in the aspects of particle size and the number of ZnO_x. Firstly, in situ XRD shows that the addition of Mn decreases the crystalline size of Cu and ZnO. When the Mn content is 2 %, the crystalline sizes of Cu and ZnO are lower than other Mn contents, which leads to the number of interfaces between Cu and ZnO in the catalyst of CZA-2%Mn is higher than other catalysts. Secondly, the in situ XPS shows that the addition of Mn effectively increases the number of the partial reduction of ZnO to metal Zn^0. The promoting effect is the most significant in CZA-2%Mn and consequently form most Cu-ZnO_x sites. Therefore, the lower size of Cu and ZnO and higher content of Zn^0 in Zn species leads to the highest number Cu-ZnO_x sites in CZA-2%Mn, which is further confirmed by N_2O titration experiment.

In situ DRIFTS shows the adsorption site of CO is the Cu-ZnO_x sites during the reaction, and the highest adsorption strength of CO is obtained in the CZA-2%Mn. H_2 dissociates on metallic Cu and then spills over the surface of ZnO to be stored [10]. In this work, CO-TPD and H_2-TPD of the spent catalysts shows the CO on the Cu-ZnO_x sites and H species stored on the surface of ZnO are the highest in CZA-2%Mn. Therefore, more surface CO and H species as well as the highest number of the Cu-ZnO_x sites are apt to promoting the reaction activity, which makes the TOF of methanol synthesis highest in CZA-2%Mn catalyst.

The water formation was proposed to accelerate the crystallization of Cu and ZnO particles in the catalyst and resulted in rapid deactivation [11]. The constant of WGS reaction close to chemical equilibrium of CZA-xMn catalyst was not changed with the increase content of Mn, indicating that the degrees of WGS reaction on different catalysts were same and their impact on the Cu and ZnO particles and methanol synthesis reaction could be negligible. Besides, the addition of Mn prevents the aggregation of the catalyst. Therefore, the decrease of the particle size and unchanged constant of WGS reaction close to chemical equilibrium consequently improve the stability of the catalyst. Finally, a suggestion for the precise design of the catalyst is decreasing the particle sizes of Cu and ZnO_x and increasing the formation of the Cu-ZnO_x.

4. Conclusion

In this paper, a series of Cu/ZnO/Al_2O_3-Mn catalysts with different Mn contents were prepared and the effects of Mn content on the catalyst structure evolution and catalytic performance in the synthesis of methanol from syngas were carried out. The reaction pathways maintain unchanged with the addition of Mn, whereas the number of Cu-ZnO_x sites active sites increase by decreasing the particle size of Cu and ZnO and increasing the content of Zn^0, and the surface CO and H species increase simultaneously, consequently forming a higher turnover frequency of methanol formation on the catalyst of Cu/ZnO/Al_2O_3-2%Mn. The unraveling the regulation of Mn in Cu-ZnO_x formation will inspire us to precisely design Cu/ZnO/Al_2O_3 catalysts with higher methanol synthesis activity.

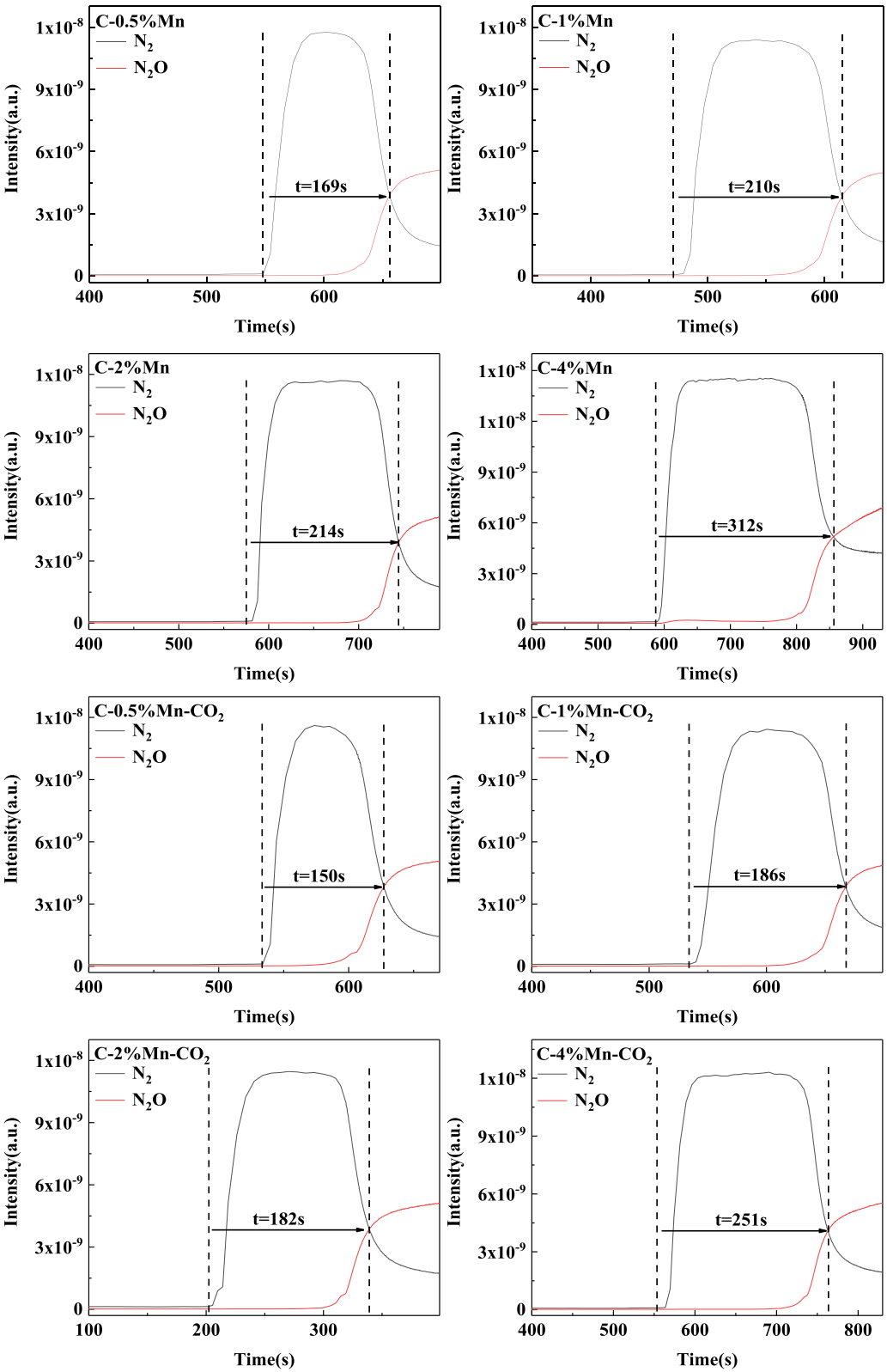

Fig. 9. N_2O titration experiment of C-xMn catalysts without CO_2 treatment (C-0.5% Mn, C-1%Mn, C-2%Mn and C-4%Mn) and after CO_2 treatment (C-0.5%Mn-CO_2, C-1%Mn-CO_2, C-2%Mn-CO_2 and C-4%Mn-CO_2).

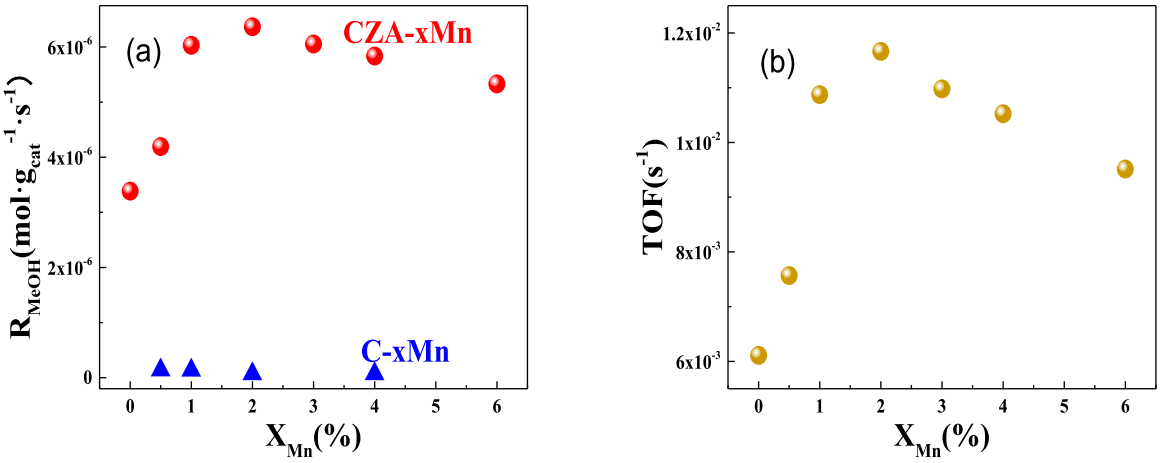

Fig. 10. Methanol formation rates over CZA-xMn and C-xMn catalysts (a), the TOF of CZA-xMn catalysts (b).

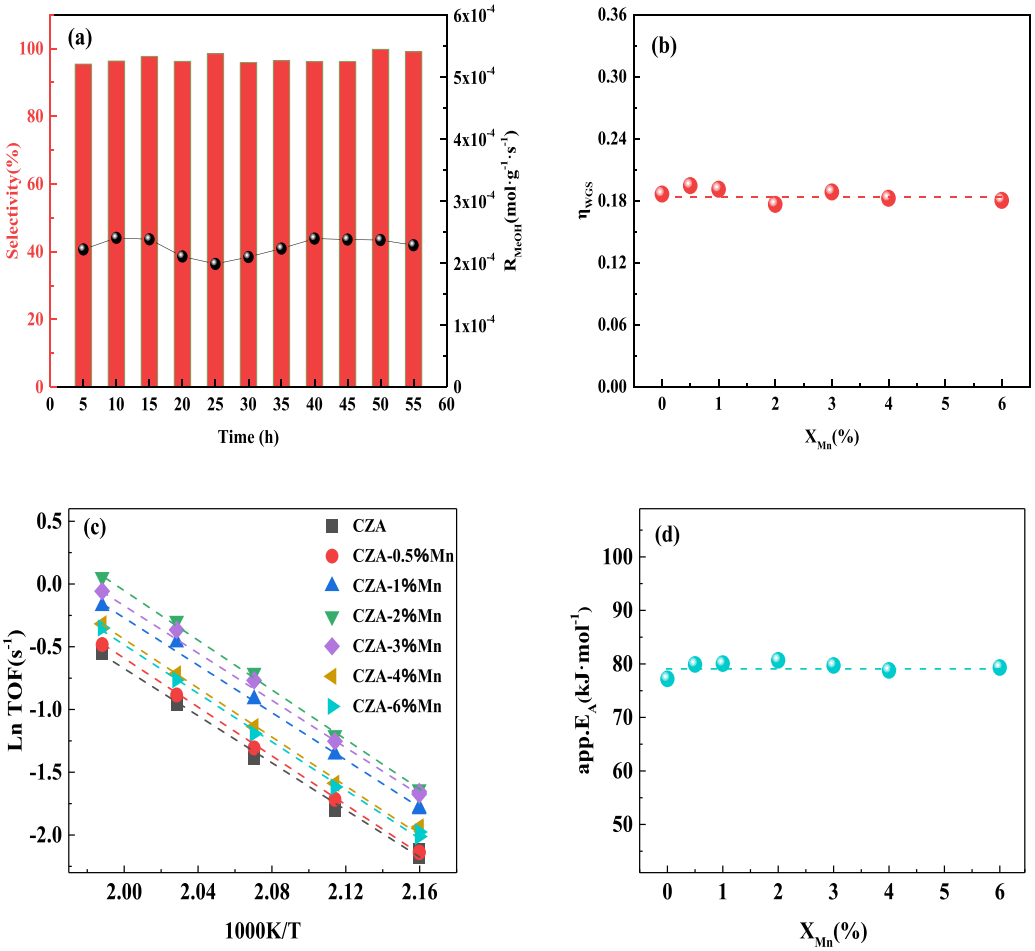

Fig. 11. (a) Catalytic performance of CZA-2%Mn catalyst for methanol synthesis from syngas for 55 h, reaction condition : 220 ℃, 1500 kPa, $H_2/CO/CO_2$ = 3/1/0.1, 48,000 mL·g_{cat}^{-1}·h^{-1}. (b) η_{WGS} spectrum of WGS reaction of CZA-xMn catalysts. (c) Arrhenius plots for methanol synthesis and (d) apparent activation energy of CZA-xMn catalysts.

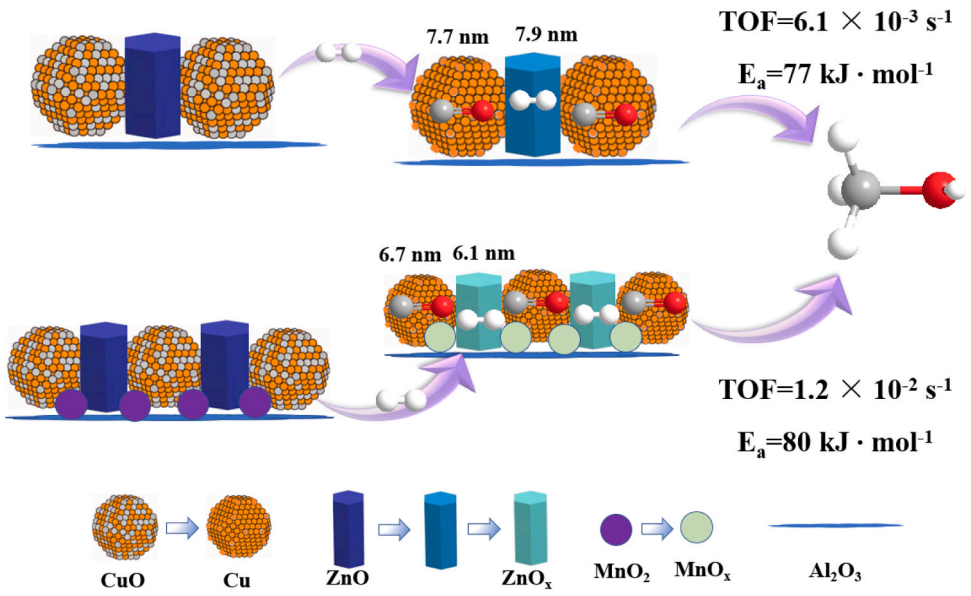

Scheme 1. The regulation of Mn in Cu-ZnO_x formation during methanol synthesis from syngas over Cu/ZnO/Al_2O_3-MnO_2 catalysts.

CRediT authorship contribution statement

Zhenzhou Zhang: Conceptualization, Methodology, Writing, Data curation, Characterization, Funding acquisition. **Sifan Cheng**: Investigation, Validation, Synthesis, Data curation, Characterization, Writing. **Wenqi Liu**: Characterization; **Baojian Chen**: Data curation. **Peng Wang**: Validation. **Jian Gao**: Characterization. **Xinhua Gao**: Characterization. **Yisheng Tan**: Validation. **Shanshan Dang**: Validation. **Weifeng Tu**: Supervision, Funding acquisition, Writing – review & editing.

Declaration of Competing Interest

The authors declare that they have no competing financial interests or personal relationships that could have appeared to influence the work reported in this paper.

Data availability

Data will be made available on request.

Acknowledgments

The authors are grateful to the National Natural Science Foundation of China (22278379, 22238003, 22208314, and 22078307), Natural Science Foundation of Henan Province (202300410432). The work is also supported by the State Key Laboratory of High-efficiency Utilization of Coal and Green Chemical Engineering (2022-K05 and 2022-K21) and the State Key Laboratory of Coal Conversion (J21–22-902).

Appendix A. Supporting information

Supplementary data associated with this article can be found in the online version at doi:10.1016/j.apcatb.2023.122985.

References

[1] P. Tian, Y.X. Wei, M. Ye, Z.M. Liu, Methanol to olefins (MTO): from fundamentals to commercialization, ACS Catal. 5 (2015) 1922–1938.
[2] Y.J. Gao, J.B.L. Liu, S. Bashir, Electrocatalysts for direct methanol fuel cells to demonstrate China's renewable energy renewable portfolio standards within the framework of the 13th five-year plan, Catal. Today 374 (2021) 135–153.
[3] G.A. Olah, Towards oil independence through renewable methanol chemistry, Angew. Chem. Int. Ed. 52 (2013) 104–107.
[4] B. Hu, Y.Z. Yin, G.L. Liu, S.L. Chen, X.L. Hong, S.C.E. Tsang, Hydrogen spillover enabled active Cu sites for methanol synthesis from CO_2 hydrogenation over Pd doped CuZn catalysts, J. Catal. 359 (2018) 17–26.
[5] Y. Yao, Y. Chang, R.Z. Huang, L.X. Zhang, E. Masanet, Environmental implications of the methanol economy in China: well-to-wheel comparison of energy and environmental emissions for different methanol fuel production pathways, J. Clean. Prod. 172 (2018) 1381–1390.
[6] H.B. Zhao, R.F. Yu, S.C. Ma, K.Z. Xu, Y. Chen, K. Jiang, Y. Fang, C.X. Zhu, X.C. Liu, Y. Tang, L.Z. Wu, Y.Q. Wu, Q.K. Jiang, P. He, Z.P. Liu, L. Tan, The role of Cu-1-O-3 species in single-atom Cu/ZrO_2 catalyst for CO_2 hydrogenation, Nat. Catal. 5 (2022) 818–831.
[7] K. Cheng, B. Gu, X.L. Liu, J.C. Kang, Q.H. Zhang, Y. Wang, Direct and highly selective conversion of synthesis gas into lower olefins: design of a bifunctional catalyst combining methanol synthesis and carbon-carbon coupling, Angew. Chem. Int. Ed. 55 (2016) 4725–4728.
[8] P.B. Rasmussen, P.M. Holmblad, T. Askgaard, C.V. Ovesen, P. Stoltze, J.K. Norskov, I. Chorkendorff, Methanol synthesis on Cu(100) from a binary gas-mixture of CO_2 and H_2, Catal. Lett. 26 (1994) 373–381.
[9] A. Alvarez, A. Bansode, A. Urakawa, A.V. Bavykina, T.A. Wezendonk, M. Makkee, J. Gascon, F. Kapteijn, Challenges in the greener production of formates/formic acid, methanol, and DME by heterogeneously catalyzed CO_2 hydrogenation processes, Chem. Rev. 117 (2017) 9804–9838.
[10] C. Tisseraud, C. Comminges, S. Pronier, Y. Pouilloux, A. Le Valant, The Cu-ZnO synergy in methanol synthesis Part 3: impact of the composition of a selective Cu@ZnOx core-shell catalyst on methanol rate explained by experimental studies and a concentric spheres model, J. Catal. 343 (2016) 106–114.
[11] S.G. Jadhav, P.D. Vaidya, B.M. Bhanage, J.B. Joshi, Catalytic carbon dioxide hydrogenation to methanol: a review of recent studies, Chem. Eng. Res. Des. 92 (2014) 2557–2567.
[12] R. Ladera, F.J. Perez-Alonso, J.M. Gonzalez-Carballo, M. Ojeda, S. Rojas, J.L. G. Fierro, Catalytic valorization of CO_2 via methanol synthesis with Ga-promoted Cu-ZnO-ZrO_2 catalysts, Appl. Catal. B-Environ. 142 (2013) 241–248.
[13] S. Ledakowicz, L. Nowicki, J. Petera, J. Niziol, P. Kowalik, A. Golebiowski, Kinetic characterisation of catalysts for methanol synthesis, Chem. Process Eng. 34 (2013) 497–506.
[14] M. Sadeghinia, A.N.K. Ghaziani, M. Rezaei, Component ratio dependent Cu/Zn/Al structure sensitive catalyst in CO_2/CO hydrogenation to methanol, Mol. Catal. 456 (2018) 38–48.
[15] V. Dasireddy, N.S. Stefancic, M. Hus, B. Likozar, Effect of alkaline earth metal oxide (MO) Cu/MO/Al_2O_3 catalysts on methanol synthesis activity and selectivity via CO_2 reduction, Fuel 233 (2018) 103–112.
[16] G.C. Chinchen, C.M. Hay, H.D. Vandervell, K.C. Waugh, The measurement of copper surface-areas by reactive frontal chromatography, J. Catal. 103 (1987) 79–86.
[17] G.C. Chinchen, K.C. Waugh, D.A. Whan, The activity and state of the copper surface in methanol synthesis catalysts, Appl. Catal. 25 (1986) 101–107.
[18] T.H. Fleisch, R.L. Mieville, Studies on the chemical-state of cu during methanol synthesis, J. Catal. 90 (1984) 165–172.
[19] B.S. Clausen, G. Steffensen, B. Fabius, J. Villadsen, R. Feidenhans'l, H. Topsce, In situ cell for combined XRD and on-line catalysis tests: studies of Cu-based water gas shift and methanol catalysts, J. Catal. 132 (1991) 524–535.

[20] S. Kuld, M. Thorhauge, H. Falsig, C.F. Elkjaer, S. Helveg, I. Chorkendorff, J. Sehested, Quantifying the promotion of Cu catalysts by ZnO for methanol synthesis, Science 352 (2016) 969–974.
[21] S. Kattel, P.J. Ramirez, J.G. Chen, J.A. Rodriguez, P. Liu, Catalysis active sites for CO_2 hydrogenation to methanol on Cu/ZnO catalysts, Science 355 (2017) 1296.
[22] T. Fujitani, J. Nakamura, The chemical modification seen in the Cu/ZnO methanol synthesis catalysts, Appl. Catal. A-Gen. 191 (2000) 111–129.
[23] V.E. Ostrovskii, Mechanisms of methanol synthesis from hydrogen and carbon oxides at Cu-Zn-containing catalysts in the context of some fundamental problems of heterogeneous catalysis, Catal. Today 77 (2002) 141–160.
[24] L.P.C. Silva, M.M. Freitas, L.E. Terra, A. Coutinho, F.B. Passos, Preparation of CuO/ZnO/Nb_2O_5 catalyst for the water-gas shift reaction, Catal. Today 344 (2020) 59–65.
[25] I. Abbas, H. Kim, C.H. Shin, S. Yoon, K.D. Jung, Differences in bifunctionality of ZnO and ZrO_2 in Cu/ZnO/ZrO_2/Al_2O_3 catalysts in hydrogenation of carbon oxides for methanol synthesis, Appl. Catal. B-Environ. 258 (2019).
[26] J. Paterson, R. Partington, M. Peacock, K. Sullivan, J. Wilson, Z.R. Xu, Elucidating the role of bifunctional cobalt-manganese catalyst interactions for higher alcohol synthesis, Eur. J. Inorg. Chem. 2020 (2020) 2312–2324.
[27] J. Paterson, M. Peacock, R. Purves, R. Partington, K. Sullivan, G. Sunley, J. Wilson, Manipulation of Fischer-Tropsch synthesis for production of higher alcohols using manganese promoters, ChemCatChem 10 (2018) 5154–5163.
[28] P.Y. Liao, C. Zhang, L.J. Zhang, Y.Z. Yang, L.S. Zhong, H. Wang, Y.H. Sun, Higher alcohol synthesis via syngas over CoMn catalysts derived from hydrotalcite-like precursors, Catal. Today 311 (2018) 56–64.
[29] G.R. Johnson, S. Werner, A.T. Bell, An investigation into the effects of Mn promotion on the activity and selectivity of Co/SiO_2 for Fischer-Tropsch synthesis: evidence for enhanced CO adsorption and dissociation, ACS Catal. 5 (2015) 5888–5903.
[30] G.L. Bezemer, P.B. Radstake, U. Falke, H. Oosterbeek, H. Kuipers, A. van Dillen, K. P. de Jong, Investigation of promoter effects of manganese oxide on carbon nanofiber-supported cobalt catalysts for Fischer-Tropsch synthesis, J. Catal. 237 (2006) 152–161.
[31] H. Blanco, S.H. Lima, V.D. Rodrigues, L.A. Palacio, A.D. Faro, Copper-manganese catalysts with high activity for methanol synthesis, Appl. Catal. A-Gen. 579 (2019) 65–74.
[32] Y.S. Tan, H.J. Xie, H.T. Cui, Y.Z. Han, B. Zhong, Modification of Cu-based methanol synthesis catalyst for dimethyl ether synthesis from syngas in slurry phase, Catal. Today 104 (2005) 25–29.
[33] J.M. Beiramar, A. Griboval-Constant, A.Y. Khodakov, Effects of metal promotion on the performance of CuZnAl catalysts for alcohol synthesis, ChemCatChem 6 (2014) 1788–1793.
[34] T.Q. Ye, Y. Ai, B. Chen, Y.W. Ye, J. Sun, L. Qin, X. Yao, Enhancement of aldehyde-water shift reaction over CuZnAl catalyst by Mn promoter, Catal. Commun. 149 (2021).
[35] G.C. Bond, S.N. Namijo, An improved procedure for estimating the metal-surface area of supported copper-catalysts, J. Catal. 118 (1989) 507–510.
[36] S.Y. Chen, J.F. Zhang, P. Wang, X.X. Wang, F.E. Song, Y.X. Bai, M. Zhang, Y.Q. Wu, H.J. Xie, Y.S. Tan, Effect of vapor-phase-treatment to CuZnZr catalyst on the reaction behaviors in CO_2 hydrogenation into methanol, ChemCatChem 11 (2019) 1448–1457.
[37] W.W. Wang, Z.P. Qu, L.X. Song, Q. Fu, Effect of the nature of copper species on methanol synthesis from CO_2 hydrogenation reaction over CuO/$Ce_{0.4}Zr_{0.6}O_2$ catalyst, Mol. Catal. 493 (2020).
[38] J. Hu, Y.Y. Li, Y.P. Zhen, M.S. Chen, H.L. Wan, In situ FTIR and ex situ XPS/HS-LEIS study of supported Cu/Al_2O_3 and Cu/ZnO catalysts for CO_2 hydrogenation, Chin. J. Catal. 42 (2021) 367–375.
[39] L.J. Liu, F. Gao, H.L. Zhao, Y. Li, Tailoring Cu valence and oxygen vacancy in Cu/TiO_2 catalysts for enhanced CO_2 photoreduction efficiency, Appl. Catal. B-Environ. 134 (2013) 349–358.
[40] L.P. Han, L. Zhang, G.F. Zhao, Y.F. Chen, Q.F. Zhang, R.J. Chai, Y. Liu, Y. Lu, Copper-fiber-structured Pd-Au-CuOx: preparation and catalytic performance in the vapor-phase hydrogenation of dimethyl oxalate to ethylene glycol, ChemCatChem 8 (2016) 1065–1073.
[41] Z.H. Li, W. Huang, Z.J. Zuo, Y.J. Song, K.C. Xie, XPS study on CuZnAl catalysts prepared by different methods for direct synthesis of dimethyl ether, Chin. J. Catal. 30 (2009) 171–177.
[42] I. Platzman, R. Brener, H. Haick, R. Tannenbaum, Oxidation of polycrystalline copper thin films at ambient conditions, J. Phys. Chem. C 112 (2008) 1101–1108.
[43] S. Velu, K. Suzuki, C.S. Gopinath, H. Yoshida, T. Hattori, XPS, XANES and EXAFS investigations of CuO/ZnO/$Al_{(2)}O_3$/ZrO_2 mixed oxide catalysts, Phys. Chem. Chem. Phys. 4 (2002) 1990–1999.
[44] H. Iwai, T. Umeki, M. Yokomatsu, C. Egawa, Methanol partial oxidation on Cu-Zn thin films grown on Ni(100) surface, Surf. Sci. 602 (2008) 2541–2546.
[45] C.H. Zhang, C. Wang, W.C. Zhan, Y.L. Guo, Y. Guo, G.Z. Lu, A. Baylet, A. Giroir-Fendler, Catalytic oxidation of vinyl chloride emission over LaMnO3 and $LaB_{0.2}Mn_{0.8}O_3$ (B = Co, Ni, Fe) catalysts, Appl. Catal. B-Environ. 129 (2013) 509–516.
[46] L.B. Hoch, T.E. Wood, P.G. O'Brien, K. Liao, L.M. Reyes, C.A. Mims, G.A. Ozin, The rational design of a single-component photocatalyst for gas-phase CO_2 reduction using both UV and visible light, Adv. Sci. 1 (2014).
[47] A. Dandekar, M.A. Vannice, Determination of the dispersion and surface oxidation states of supported Cu catalysts, J. Catal. 178 (1998) 621–639.
[48] M. Behrens, F. Studt, I. Kasatkin, S. Kuhl, M. Havecker, F. Abild-Pedersen, S. Zander, F. Girgsdies, P. Kurr, B.L. Kniep, M. Tovar, R.W. Fischer, J.K. Norskov, R. Schlogl, The active site of methanol synthesis over Cu/ZnO/Al_2O_3 industrial catalysts, Science 336 (2012) 893–897.
[49] V. Schott, H. Oberhofer, A. Birkner, M.C. Xu, Y.M. Wang, M. Muhler, K. Reuter, C. Woll, Chemical activity of thin oxide layers: strong interactions with the support yield a new thin-film phase of ZnO, Angew. Chem. Int. Ed. 52 (2013) 11925–11929.
[50] H. Li, X.F. Weng, Z.Y. Tang, H. Zhang, D. Ding, M.S. Chen, H.L. Wan, Evidence of the encapsulation model for strong metal-support interaction under oxidized conditions: a case study on TiOx/Pt(111) for CO oxidation by in situ wide spectral range infrared reflection adsorption spectroscopy, ACS Catal. 8 (2018) 10156–10163.
[51] Y.P. Zheng, L.H. Zhang, S.L. Wang, D. Ding, H. Zhang, M.S. Chen, H.L. Wan, Synergistic effects of VOx-Pt probed by the oxidation of propane on VOx/Pt(111), Langmuir 29 (2013) 9090–9097.
[52] E.D. Batyrev, N.R. Shiju, G. Rothenberg, Exploring the activated state of Cu/ZnO (0001)-Zn, a model catalyst for methanol synthesis, J. Phys. Chem. C 116 (2012) 19335–19341.
[53] X.S. Dong, F. Li, N. Zhao, F.K. Xiao, J.W. Wang, Y.S. Tan, CO_2 hydrogenation to methanol over Cu/ZnO/ZrO_2 catalysts prepared by precipitation-reduction method, Appl. Catal. B-Environ. 191 (2016) 8–17.
[54] X. Dong, H.B. Zhang, G.D. Lin, Y.Z. Yuan, K.R. Tsai, Highly active CNT-promoted Cu-ZnO-Al_2O_3 catalyst for methanol synthesis from H_2/CO/CO_2, Catal. Lett. 85 (2003) 237–246.
[55] A. Le Valant, C. Comminges, C. Tisseraud, C. Canaff, L. Pinard, Y. Pouilloux, The Cu-ZnO synergy in methanol synthesis from CO_2, Part 1: origin of active site explained by experimental studies and a sphere contact quantification model on Cu plus ZnO mechanical mixtures, J. Catal. 324 (2015) 41–49.
[56] K.Z. Li, J.G.G. Chen, CO_2 hydrogenation to methanol over ZrO_2-containing catalysts: insights into ZrO_2 induced synergy, ACS Catal. 9 (2019) 7840–7861.
[57] P. Gao, F. Li, H.J. Zhan, N. Zhao, F.K. Xiao, W. Wei, L.S. Zhong, H. Wang, Y.H. Sun, Influence of Zr on the performance of Cu/Zn/Al/Zr catalysts via hydrotalcite-like precursors for CO_2 hydrogenation to methanol, J. Catal. 298 (2013) 51–60.
[58] I.U. Din, M.S. Shaharun, M.A. Alotaibi, A.I. Alharthi, A. Naeem, Recent developments on heterogeneous catalytic CO_2 reduction to methanol, J. CO_2 Util. 34 (2019) 20–33.
[59] S. Natesakhawat, J.W. Lekse, J.P. Baltrus, P.R. Ohodnicki, B.H. Howard, X.Y. Deng, C. Matranga, Active sites and structure-activity relationships of copper-based catalysts for carbon dioxide hydrogenation to methanol, ACS Catal. 2 (2012) 1667–1676.
[60] D.B. Clarke, A.T. Bell, An infrared study of methanol synthesis from CO_2 on clean and potassium-promoted Cu/SiO_2, J. Catal. 154 (1995) 314–328.
[61] J. Yoshihara, S.C. Parker, A. Schafer, C.T. Campbell, Methanol synthesis and reverse water-gas shift kinetics over clean polycrystalline copper, Catal. Lett. 31 (1995) 313–324.
[62] J.C. Medina, M. Figueroa, R. Manrique, J.R. Pereira, P.D. Srinivasan, J.J. Bravo-Saurez, V.G.B. Medrano, R. Jimenez, A. Karelovic, Catalytic consequences of Ga promotion on Cu for CO_2 hydrogenation to methanol, Catal. Sci. Technol. 7 (2017) 3375–3387.